Steady-State Entanglement in the Nuclear Spin Dynamics of a Double Quantum Dot

M. J. A. Schuetz,[1] E. M. Kessler,[2,3] L. M. K. Vandersypen,[4] J. I. Cirac,[1] and G. Giedke[1]

[1]*Max-Planck-Institut für Quantenoptik, Hans-Kopfermann-Straße 1, 85748 Garching, Germany*
[2]*Physics Department, Harvard University, Cambridge, Massachusetts 02318, USA*
[3]*ITAMP, Harvard-Smithsonian Center for Astrophysics, Cambridge, Massachusetts 02138, USA*
[4]*Kavli Institute of NanoScience, TU Delft, P.O. Box 5046, 2600 GA Delft, The Netherlands*

(Received 17 August 2013; published 9 December 2013)

We propose a scheme for the deterministic generation of steady-state entanglement between the two nuclear spin ensembles in an electrically defined double quantum dot. Because of quantum interference in the collective coupling to the electronic degrees of freedom, the nuclear system is actively driven into a two-mode squeezedlike target state. The entanglement buildup is accompanied by a self-polarization of the nuclear spins towards large Overhauser field gradients. Moreover, the feedback between the electronic and nuclear dynamics leads to multistability and criticality in the steady-state solutions.

DOI: 10.1103/PhysRevLett.111.246802 PACS numbers: 73.21.La, 03.67.Bg, 42.50.Dv, 73.63.Kv

Entanglement is a key ingredient to applications in quantum information science. In practice, however, it is very fragile and is often destroyed by the undesired coupling of the system to its environment; hence, robust ways to prepare entangled states are called for. Schemes that exploit open system dynamics to prepare them as steady states are particularly promising [1–5]. Here, we investigate such a scheme in quantum information architectures using spin qubits in quantum dots [6,7]. In these systems, a great deal of research has been directed towards the complex interplay between electron and nuclear spins [8–15], with the ultimate goal of turning the nuclear spins from the dominant source of decoherence [16–19] into a useful resource [20–23]. The creation of entanglement between nuclear spins constitutes a pivotal element towards these goals.

In this work, we propose a scheme for the dissipative preparation of steady-state entanglement between the two nuclear spin ensembles in a double quantum dot (DQD) in the Pauli-blockade regime [6,24]. The entanglement arises from an interference between different hyperfine-induced processes lifting the Pauli blockade. This becomes possible by suitably engineering the effective electronic environment, which ensures a *collective* coupling of electrons and nuclei (i.e., each flip can happen either in the left or the right QD and no which-way information is leaked), and that just two such processes with a common entangled stationary state are dominant. Engineering of the electronic system via external gate voltages facilitates the control of the desired steady-state properties. Exploiting the separation of electronic and nuclear time scales allows us to derive a quantum master equation in which the interference effect becomes apparent: It features nonlocal jump operators which drive the nuclear system into an entangled steady state of EPR-type [5]. Since the entanglement is actively stabilized by the dissipative dynamics, our approach is inherently robust against weak random perturbations [1–5]. The entanglement buildup is accompanied by a self-polarization of the nuclear system towards large Overhauser (OH) field gradients if a small initial gradient is provided. Upon surpassing a certain threshold value of this field the nuclear dynamics turn self-polarizing, and drive the system to even larger gradients. Entanglement is then generated in the quantum fluctuations around these macroscopic nuclear polarizations. Furthermore, feedback between electronic and nuclear dynamics leads to multistability and criticality in the steady-state solutions.

We consider a DQD in the Pauli-blockade regime [6,24]; see Fig. 1. A source-drain bias across the device induces electron transport via the cycle $(0,1) \rightarrow (1,1) \rightarrow (0,2) \rightarrow (0,1)$. Here, (m, n) refers to a configuration with $m(n)$ electrons in the left (right) dot, respectively. The only energetically accessible (0, 2) state is the localized singlet, $|S_{02}\rangle$. Then, by the Pauli principle, the interdot charge transition $(1,1) \rightarrow (0,2)$ is allowed only for the (1, 1) spin singlet $|S_{11}\rangle = (|\Uparrow\Downarrow\rangle - |\Downarrow\Uparrow\rangle)/\sqrt{2}$, while the spin-triplet states $|T_{\pm}\rangle$ and $|T_0\rangle = (|\Uparrow\Downarrow\rangle + |\Downarrow\Uparrow\rangle)/\sqrt{2}$ are blocked. Including a homogeneous Zeeman splitting ω_0 and a magnetic gradient Δ, both oriented along $\hat{z}$, the DQD within the relevant two-electron subspace is then described by the effective Hamiltonian ($\hbar = 1$)

$$H_{\mathrm{el}} = \omega_0(S_1^z + S_2^z) + \Delta(S_2^z - S_1^z) - \epsilon|S_{02}\rangle\langle S_{02}| + t(|\Uparrow\Downarrow\rangle\langle S_{02}| - |\Downarrow\Uparrow\rangle\langle S_{02}| + \mathrm{H.c.}), \quad (1)$$

where ϵ refers to the relative interdot energy detuning between the left and right dots and t describes interdot electron tunneling in the Pauli-blockade regime.

The spin blockade inherent to H_{el} can be lifted, e.g., by the hyperfine (HF) interaction with nuclear spins in the host environment. The electronic spins $\vec{S}_i$ confined in either of the two dots ($i = 1, 2$) are coupled to two different sets of nuclei $\{\sigma_{i,j}^{\alpha}\}$ via the isotropic Fermi contact interaction [25]

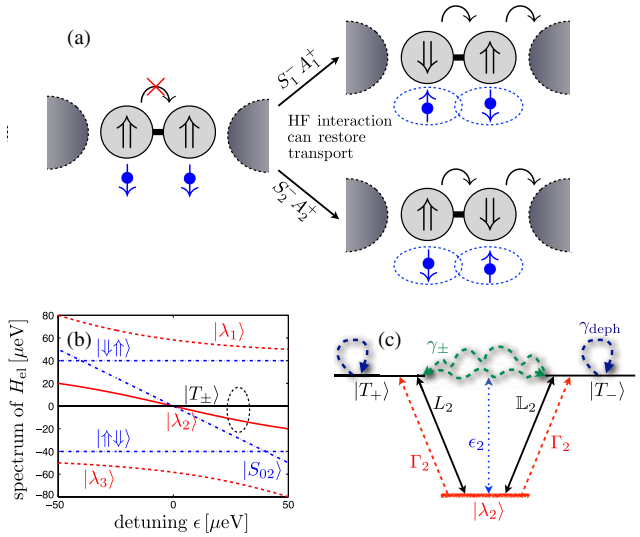

FIG. 1 (color online). (a) Schematic illustration of nuclear entanglement generation via electron transport. Whenever the Pauli blockade is lifted via the HF interaction with the nuclear spins, a nuclear flip can occur in either of the two dots. The local nature of the HF interaction is masked by the nonlocal character of the electronic level $|\lambda_2\rangle$. (b) Spectrum of H_{el} for $\Delta = 40$ μeV and $t = 30$ μeV. The three eigenstates $|\lambda_k\rangle$ are displayed in red. The triplets $|T_\pm\rangle$ are degenerate for $\omega_0 = 0$. In this setting, lifting of the spin blockade due to HF interaction is predominantly mediated by the nonlocal jump operators required for two-mode squeezing, namely, L_2 and $\mathbb{L}_2$. The ellipse refers to a potential operational area of our scheme. (c) The resulting effective three-level system $\{|T_\pm\rangle, |\lambda_2\rangle\}$ including coherent HF coupling and the relevant dissipative processes: $|\lambda_2\rangle$ decays according to its overlap with $|S_{02}\rangle$ with an effective decay rate $\Gamma_2 = |\langle\lambda_2|S_{02}\rangle|^2\Gamma$ [43]. Within this three-level subspace, purely electronic Pauli-blockade lifting mechanisms like cotunneling or spin-orbital effects result in effective dephasing and dissipative mixing rates, labeled as γ_{deph} and $\gamma_\pm$, respectively.

$$H_{HF} = \frac{a_{HF}}{2}\sum_{i=1,2}(S_i^+A_i^- + S_i^-A_i^+) + a_{HF}\sum_{i=1,2}S_i^zA_i^z. \quad (2)$$

Here, S_i^α and $A_i^\alpha = \sum_j a_{i,j}\sigma_{i,j}^\alpha$ for $\alpha = \pm, z$ denote electron and collective nuclear spin operators, and $a_{i,j}$ defines the unitless HF coupling constant between the electron spin in dot i and the jth nucleus: $\sum_{j=1}^{N_i} a_{i,j} = N$, where $N = (N_1 + N_2)/2 \sim 10^6$ refers to the average number of nuclei per dot. The individual nuclear spin operators $\sigma_{i,j}^\alpha$ are assumed to be spin-$\frac{1}{2}$ and we neglect the nuclear Zeeman and dipole-dipole terms [25]. The second term in Eq. (2) can be split into an effective nuclear magnetic field and residual quantum fluctuations, $H_{zz} = a_{HF}\sum_{i=1,2}S_i^z\delta A_i^z$, where $\delta A_i^z = A_i^z - \langle A_i^z\rangle_t$. The (time-dependent) semiclassical OH field exhibits a homogeneous $\bar{\omega}_{OH} = (a_{HF}/2)\times(\langle A_1^z\rangle_t + \langle A_2^z\rangle_t)$ and inhomogeneous component $\Delta_{OH} = (a_{HF}/2)(\langle A_2^z\rangle_t - \langle A_1^z\rangle_t)$, which can be absorbed into the definitions of ω_0 and Δ in Eq. (1) as $\omega_0 = \bar{\omega}_{OH} + \omega_{ext}$ and $\Delta = \Delta_{OH} + \Delta_{ext}$, respectively. For now, we assume the symmetric situation of vanishing external fields $\omega_{ext} = \Delta_{ext} = 0$ [26]. Thus, ω_0 and Δ are dynamic variables depending on the nuclear polarizations.

The flip-flop dynamics, given by the first term in Eq. (2), and the OH fluctuations described by H_{zz} can be treated perturbatively with respect to the effective electronic Hamiltonian H_{el}. Its eigenstates within the $S_{tot}^z = S_1^z + S_2^z = 0$ subspace can be expressed as $|\lambda_k\rangle = \mu_k|\Uparrow\Downarrow\rangle + \nu_k|\Downarrow\Uparrow\rangle + \kappa_k|S_{02}\rangle$ $(k = 1, 2, 3)$ with corresponding eigenenergies ϵ_k. For $t \gg \omega_0$, g_{HF}, where $g_{HF} = \sqrt{N}a_{HF}$, $|\lambda_{1,3}\rangle$ are far detuned, and the electronic subsystem can be simplified to an effective three-level system comprising the levels $\{|T_\pm\rangle, |\lambda_2\rangle\}$. Effects arising due to the presence of $|\lambda_{1,3}\rangle$ will be discussed below. Within this reduced scheme, H_{ff} reads

$$H_{ff} = \frac{a_{HF}}{2}[L_2|\lambda_2\rangle\langle T_+| + \mathbb{L}_2|\lambda_2\rangle\langle T_-| + \text{H.c.}], \quad (3)$$

where the *nonlocal* nuclear operators $L_2 = \nu_2A_1^+ + \mu_2A_2^+$ and $\mathbb{L}_2 = \mu_2A_1^- + \nu_2A_2^-$ are associated with lifting the Pauli blockade from $|T_+\rangle$ and $|T_-\rangle$ via $|\lambda_2\rangle$, respectively. They can be controlled via the external parameters t and ϵ defining the amplitudes μ_2 and ν_2.

The dynamical evolution of the system is described in terms of a Markovian master equation for the reduced density matrix of the DQD system ρ describing the relevant electronic and nuclear degrees of freedom [11]. Besides the HF dynamics described above, it accounts for other purely electronic mechanisms like, e.g., cotunneling. These effects and their implications for the nuclear dynamics are described in [26] and lead to effective decay and dephasing processes in the $T_\pm$ subspace with rates $\gamma_\pm$, γ_{deph}; see Fig. 1(c). For fast electronic dynamics ($\gamma_\pm$, $\gamma_{deph} \gg g_{HF}$) and a sufficiently high gradient $\Delta \gtrsim 3$ μeV (see [26]), the hybridized electronic level $|\lambda_2\rangle$ exhibits a significant overlap with the localized singlet $|S_{02}\rangle$ and the electronic subsystem settles in the desired quasisteady state, $\rho_{ss}^{el} = (|T_+\rangle\langle T_+| + |T_-\rangle\langle T_-|)/2$, on a time scale much shorter than the nuclear dynamics. One can then adiabatically eliminate all electronic coordinates yielding a coarse-grained equation of motion for the nuclear density matrix $\sigma = \mathrm{Tr}_{el}[\rho]$, where $\mathrm{Tr}_{el}[\ldots]$ denotes the trace over the electronic degrees of freedom: $\dot{\sigma} = \mathcal{L}_{id}[\sigma] + \mathcal{L}_{nid}[\sigma]$. Here, the first dominant term describes the desired nuclear squeezing dynamics

$$\mathcal{L}_{id}[\sigma] = \frac{\gamma}{2}[\mathcal{D}[L_2]\sigma + \mathcal{D}[\mathbb{L}_2]\sigma] + i\frac{\delta}{2}([L_2^\dagger L_2, \sigma] + [\mathbb{L}_2^\dagger\mathbb{L}_2, \sigma]), \quad (4)$$

where $\mathcal{D}[c]\rho = c\rho c^\dagger - \frac{1}{2}\{c^\dagger c, \rho\}$. It arises from coupling to the level $|\lambda_2\rangle$, while $\mathcal{L}_{nid}[\sigma]$ results from coupling to the far detuned levels $|\lambda_{1,3}\rangle$ and OH fluctuations described by H_{zz} [26]. Here, γ and δ refer to a HF-mediated decay rate and Stark shift, respectively, [27].

Pure stationary solutions $|\xi_{ss}\rangle$ associated with the dynamics generated by Eq. (4) can be obtained from the

dark-state condition $L_2|\xi_{ss}\rangle = \mathbb{L}_2|\xi_{ss}\rangle = 0$. First, we consider the limit of equal dot sizes ($N_1 = N_2$) and uniform HF coupling ($a_{i,j} = N/N_i$) and generalize our results later. The nuclear system can be described via Dicke states $|J_i, k_i\rangle$, where $k_i = 0, 1, \ldots, 2J_i$ and J_i refer to the spin-$\hat{z}$ projection and total spin quantum numbers, respectively. For $J_1 = J_2 = J$, one readily checks that the dark-state condition is satisfied by the (unnormalized) pure state $|\xi_{ss}\rangle = \sum_{k=0}^{2J} \xi^k |J, k\rangle \otimes |J, 2J - k\rangle$, representing an entangled state closely similar to the two-mode squeezed state [26]. The parameter $\xi = -\nu_2/\mu_2$ quantifies the entanglement and polarization of the nuclear system. $|\xi| < 1$ ($|\xi| > 1$) corresponds to states of large positive (negative) OH gradients, respectively. The system is invariant under the symmetry transformation ($\mu_2 \leftrightarrow \nu_2$, $A^z_{1,2} \to -A^z_{1,2}$) which gives rise to a bistability in the steady state, as for every solution with positive OH gradient ($\Delta > 0$), we find another one with $\Delta < 0$.

For a given $|\xi| \neq 1$, the individual nuclear polarizations in the state $|\xi_{ss}\rangle$ approach one as we increase the system size J, and we can describe the system dynamics in the vicinity of the respective steady state in the framework of a Holstein-Primakoff (HP) transformation [28]. This allows for a detailed analysis of the nuclear dynamics including perturbative effects from the processes described by $\mathcal{L}_{nid}$. The collective nuclear spins $I^\alpha_i = \sum_j \sigma^\alpha_{i,j}$ are mapped to bosonic operators [29] and the (unique) ideal steady state is well known to be a two-mode squeezed state [5,26] which represents $|\xi_{ss}\rangle$ within the HP picture. Since in the bosonic case the modulus of ξ is confined to $|\xi| < 1$, the HP analysis refers to one of the two symmetric steady-state solutions mentioned above. Within the HP approximation the dynamics generated by $\dot{\sigma} = \mathcal{L}_{id}[\sigma] + \mathcal{L}_{nid}[\sigma]$ are quadratic in the new bosonic creation and annihilation operators. Therefore, the nuclear dynamics are purely Gaussian and exactly solvable. The generation of entanglement can be certified via the EPR entanglement condition [5,30], $\Delta_{EPR} < 1$, where $\Delta_{EPR} = [\mathrm{var}(I^x_1 + I^x_2) + \mathrm{var}(I^y_1 + I^y_2)]/(|\langle I^z_1\rangle| + |\langle I^z_2\rangle|)$. While $\Delta_{EPR} \geq 1$ for separable states, the ideal dynamics $\mathcal{L}_{id}$ drive the nuclear spins into an EPR state with $\Delta^{id}_{EPR} = (1 - |\xi|)/(1 + |\xi|) < 1$. As illustrated in Fig. 2, we numerically find that the generation of steady-state entanglement persists even for asymmetric dot sizes of $\sim$20%, classical uncertainty in the total spins J_i [31], and the undesired terms $\mathcal{L}_{nid}$. When tuning t from 10 μeV to 35 μeV, the squeezing parameter $|\xi|$ increases from $\sim$0.2 to $\sim$0.6, respectively. For $|\xi| \approx 0.2$, we obtain a relatively high fidelity $\mathcal{F}$ with the ideal two-mode squeezed state, close to 80%. For stronger squeezing, the target state becomes more susceptible to the undesired noise terms, first leading to a reduction of $\mathcal{F}$ and eventually to a breakdown of the HP approximation. The associated critical behavior can be understood in terms of a dissipative phase transition [28,32].

We now turn to the experimental realization of our scheme [26]: In the analysis above, we discussed the idealized case of uniform HF coupling. However, our scheme also works for nonuniform coupling, provided that the two dots are sufficiently similar: If the coupling is completely inhomogeneous, that is $a_{i,j} \neq a_{i,k}$ for all $j \neq k$, but the two QDs are identical ($a_{1,j} = a_{2,j} \forall\ j = 1, \ldots, N_1 \equiv N_2$), Eq. (4) supports a *unique pure entangled* stationary state. Up to normalization, it reads $|\xi_{ss}\rangle = \otimes_{j=1}^{N} |\xi\rangle_j$, where $|\xi\rangle_j = |\downarrow_j, \uparrow_j\rangle + \xi|\uparrow_j, \downarrow_j\rangle$ is an entangled state of two nuclear spins belonging to different nuclear ensembles [33]. $|\xi_{ss}\rangle$ features a (large) polarization gradient $\Delta_{I^z} = \langle I^z_2\rangle - \langle I^z_1\rangle = N(1 - \xi^2)/(1 + \xi^2)$.

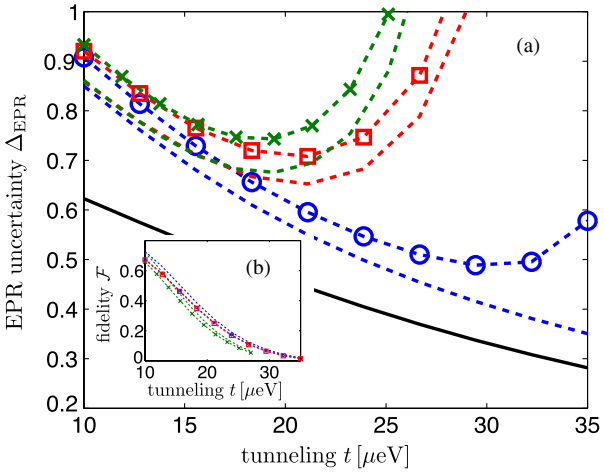

FIG. 2 (color online). Steady-state entanglement between the two nuclear spin ensembles quantified via (a) the EPR uncertainty Δ_{EPR} and (b) fidelity $\mathcal{F}$ of the nuclear steady state with the two-mode squeezed target state. The black solid curve refers to the idealized setting where the undesired HF coupling to $|\lambda_{1,3}\rangle$ has been ignored and where $J_1 = J_2 = pJ_{max}$, $p = 0.8$, and $N_1 = N_2 = 2J_{max} = 10^6$, corresponding to $\Delta_{OH} = 40$ μeV. The blue-dashed line then also takes into account coupling to $|\lambda_{1,3}\rangle$ while the red-dashed curve, in addition, accounts for an asymmetric dot size: $N_2 = 0.8N_1 = 8 \times 10^5$. The amount of entanglement decreases for a smaller nuclear polarization: $p = 0.7$ (green dashed curve). Classical uncertainty (symbols) in the total spin J_i quantum numbers leads to less entanglement, but does not destroy it. Here, we have set the range of the distribution to $\Delta_{J_i} = 50\sqrt{N_i}$. Other numerical parameters: $\omega_0 = 0$, $\Gamma = 25$ μeV, $\epsilon = 30$ μeV, and $\gamma_\pm + \gamma_{deph}/2 = 1$ μeV.

The buildup of a large OH gradient is corroborated within a semiclassical calculation which neglects correlations among the nuclear spins [26]. This is valid on time scales that are long compared to nuclear dephasing mechanisms [14,34,36]. Assuming equal dot sizes, $N_1 = N_2 = N$, we use a semiclassical factorization scheme [36] resulting in decoupled equations of motion for the two nuclear polarization variables $\langle I^z_1\rangle_t$ and $\langle I^z_2\rangle_t$ [37]. In particular, Δ_{I^z} evolves as

$$\frac{d}{dt}\Delta_{I^z} = -\gamma_{eff}\left[\Delta_{I^z} - N\frac{\chi}{\gamma_{eff}}\right], \tag{5}$$

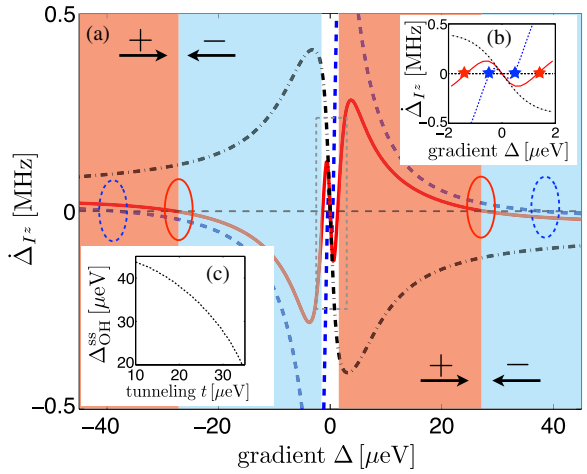

FIG. 3 (color online). Semiclassical solution to the nuclear polarization dynamics. (a) Instantaneous nuclear polarization rate $\dot{\Delta}_{I^z}$ as a function of the gradient Δ for $t = 20\ \mu$eV (blue dashed), $t = 30\ \mu$eV (red solid), and $t = 50\ \mu$eV (black dash-dotted). FPs are found at $\dot{\Delta}_{I^z} = 0$. The ovals mark stable high-gradient steady-state solutions. The background coloring refers to the sign of $\dot{\Delta}_{I^z}$ (for $t = 30\ \mu$eV) which determines the stable FP the nuclear system is attracted to (see arrows). (b) Zoom-in of (a) into the low-gradient regime: The unpolarized FP lies at $\Delta = 0$, whereas critical, instable points $\Delta_{\mathrm{OH}}^{\mathrm{crt}}$ (marked by stars) can be identified with $\dot{\Delta}_{I^z} = 0$ and $d\dot{\Delta}_{I^z}/d\Delta > 0$. (c) Stable high-polarization FPs $\Delta_{\mathrm{OH}}^{\mathrm{ss}}$ (see ovals) as a function of t; for $t \approx 10\ \mu$eV we obtain a nuclear polarization of $\sim$90%. Other numerical parameters: $\Gamma = 25\ \mu$eV, $\epsilon = 30\ \mu$eV, $\gamma_{\pm} = 0.3\ \mu$eV, and $\gamma_{\mathrm{deph}} = 0.5\ \mu$eV.

where the HF-mediated depolarization γ_{eff} and pumping rate χ (see [26] for their connection to microscopic parameters) depend on the gradient Δ defined in Eq. (1), in particular on the OH gradient $\Delta_{\mathrm{OH}} \propto \Delta_{I^z}$. The electron-nuclear feedback loop can then be closed self-consistently by identifying steady-state solutions of Eq. (5) in which the parameter Δ is provided by the nuclear OH gradient only. The instantaneous polarization rate $\dot{\Delta}_{I^z}$, given in Eq. (5), is displayed in Fig. 3 as a function of Δ, with the electronic subsystem in its respective steady state, yielding a nonlinear equation for the nuclear equilibrium polarizations. Stable fixed points (FPs) are determined by $\dot{\Delta}_{I^z} = 0$ and $d\dot{\Delta}_{I^z}/d\Delta < 0$ as opposed to instable ones where $d\dot{\Delta}_{I^z}/d\Delta > 0$ [13,15,38]. We can identify parameter regimes in which the nuclear system features three FPs which are interspersed by two instable points. Two of the stable FPs are high-polarization solutions of opposite sign, supporting a macroscopic OH gradient, while one is the trivial, zero polarization solution. If the initial gradient lies outside the instable points, the system turns self-polarizing and the OH gradient approaches a highly polarized FP. For typical parameter values we estimate that the OH gradient at the instable points is $\approx$ (1–2) μeV; compare Fig. 3(b). This comparatively moderate initial gradient could be achieved via, e.g., a nanomagnet [39,40] or alternative dynamic nuclear polarization schemes [14,20,35,41].

Next, we address the effects of weak nuclear interactions: First, we have neglected nuclear dipole-dipole interactions. However, we estimate the time scale for the entanglement creation as $t^* = \hbar/N\gamma \lesssim 10\ \mu$s which is fast compared to typical nuclear decoherence times, recently measured to be $\sim$1 ms in vertical DQDs [35]. Thus, it should be possible to create entanglement between the two nuclear spin ensembles faster than it gets disrupted by dipole-dipole interactions among the nuclei. Second, we have disregarded nuclear Zeeman terms since our scheme requires no external homogeneous magnetic field for sufficiently strong tunneling t [42].

Finally, entanglement could be detected by measuring the OH shift in each dot separately [6]; in combination with NMR techniques to rotate the nuclear spins [8] we can obtain all spin components and their variances which are sufficient to verify the presence of entanglement (similar to the proposal [9]).

To conclude, we have presented a scheme for the dissipative entanglement generation among the two nuclear spin ensembles in a DQD. This may provide a long-lived, solid-state entanglement resource and a new route for nuclear-spin-based information storage and manipulation.

We acknowledge support by the DFG within SFB 631, the Cluster of Excellence NIM and the project MALICIA within the 7th Framework Programme for Research of the European Commission, under FET-Open Grant No. 265522. E. M. K. acknowledges support by the Harvard Quantum Optics Center and the Institute for Theoretical Atomic and Molecular Physics. L. V. acknowledges support by the Dutch Foundation for Fundamental Research on Matter (FOM).

[1] B. Kraus and J. I. Cirac, Phys. Rev. Lett. **92**, 013602 (2004).
[2] F. Verstraete, M. M. Wolf, and J. I. Cirac, Nat. Phys. **5**, 633 (2009).
[3] S. Diehl, A. Micheli, A. Kantian, B. Kraus, H. P. Büchler, and P. Zoller, Nat. Phys. **4**, 878 (2008).
[4] R. Sanchez and G. Platero, Phys. Rev. B **87**, 081305(R) (2013).
[5] C. A. Muschik, E. S. Polzik, and J. I. Cirac, Phys. Rev. A **83**, 052312 (2011); H. Krauter, C. A. Muschik, K. Jensen, W. Wasilewski, J. M. Petersen, J. I. Cirac, and E. S. Polzik, Phys. Rev. Lett. **107**, 080503 (2011).
[6] R. Hanson, J. R. Petta, S. Tarucha, and L. M. K. Vandersypen, Rev. Mod. Phys. **79**, 1217 (2007).
[7] D. D. Awschalom, N. Smarth, and D. Loss, *Semiconductor Spintronics and Quantum Computation* (Springer, New York, 2002).
[8] E. A. Chekhovich, M. N. Makhonin, A. I. Tartakovskii, A. Yacoby, H. Bluhm, K. C. Nowack, and L. M. K. Vandersypen, Nat. Mater. **12**, 494 (2013).

[9] M. S. Rudner, L. M. K. Vandersypen, V. Vuletic, and L. S. Levitov, Phys. Rev. Lett. **107**, 206806 (2011).

[10] M. S. Rudner, F. H. L. Koppens, J. A. Folk, L. M. K. Vandersypen, and L. S. Levitov, Phys. Rev. B **84**, 075339 (2011).

[11] M. J. A. Schuetz, E. M. Kessler, J. I. Cirac, and G. Giedke, Phys. Rev. B **86**, 085322 (2012).

[12] K. Ono and S. Tarucha, Phys. Rev. Lett. **92**, 256803 (2004).

[13] I. T. Vink, K. C. Nowack, F. H. L. Koppens, J. Danon, Y. V. Nazarov, and L. M. K. Vandersypen, Nat. Phys. **5**, 764 (2009).

[14] M. Gullans, J. J. Krich, J. M. Taylor, H. Bluhm, B. I. Halperin, C. M. Marcus, M. Stopa, A. Yacoby, and M. D. Lukin, Phys. Rev. Lett. **104**, 226807 (2010).

[15] J. Danon, I. Vink, F. Koppens, K. Nowack, L. Vandersypen, and Yu. Nazarov, Phys. Rev. Lett. **103**, 046601 (2009).

[16] A. C. Johnson, J. R. Petta, J. M. Taylor, A. Yacoby, M. D. Lukin, C. M. Marcus, M. P. Hanson, and A. C. Gossard, Nature (London) **435**, 925 (2005).

[17] F. H. L. Koppens *et al.*, Science **309**, 1346 (2005).

[18] A. V. Khaetskii, D. Loss, and L. Glazman, Phys. Rev. Lett. **88**, 186802 (2002).

[19] H. Bluhm, S. Foletti, I. Neder, M. Rudner, D. Mahalu, V. Umansky, and A. Yacoby, Nat. Phys. **7**, 109 (2010).

[20] S. Foletti, H. Bluhm, D. Mahalu, V. Umansky, and A. Yacoby, Nat. Phys. **5**, 903 (2009).

[21] J. M. Taylor, C. M. Marcus, and M. D. Lukin, Phys. Rev. Lett. **90**, 206803 (2003).

[22] W. M. Witzel and S. Das Sarma, Phys. Rev. B **76**, 045218 (2007).

[23] H. Ribeiro, J. R. Petta, and G. Burkard, Phys. Rev. B **82**, 115445 (2010).

[24] K. Ono, D. G. Austing, Y. Tokura, and S. Tarucha, Science **297**, 1313 (2002).

[25] J. Schliemann, A. Khaetskii, and Daniel Loss, J. Phys. Condens. Matter **15**, R1809 (2003).

[26] See Supplemental Material at http://link.aps.org/supplemental/10.1103/PhysRevLett.111.246802 for further details regarding the Master equation, the ideal nuclear steady state, the HP transformation, the semiclassical analysis and a summary of the experimental requirements.

[27] Microscopically, γ and δ are given by $\gamma = a_{\mathrm{HF}}^2\tilde{\Gamma}/2[\epsilon_2^2 + \tilde{\Gamma}^2]$ and $\delta = (\epsilon_2/2\tilde{\Gamma})\gamma$, respectively. Here, $\tilde{\Gamma} = \Gamma_2 + \gamma_\pm/2 + \gamma_{\mathrm{deph}}/4$.

[28] E. M. Kessler, G. Giedke, A. Imamoglu, S. F. Yelin, M. D. Lukin, and J. I. Cirac, Phys. Rev. A **86**, 012116 (2012).

[29] Here, we consider the subspace with large collective spin quantum numbers, $J_i \sim \mathcal{O}(N/2)$. The zeroth-order HP mapping can be justified self-consistently, provided that the occupations in the bosonic modes are small compared to $2J_i$.

[30] M. G. Raymer, A. C. Funk, B. C. Sanders, and H. deGuise, Phys. Rev. A **67**, 052104 (2003).

[31] We average over an uniform distribution of $\{J_1, J_2\}$ subspaces with a range of $\Delta_{J_i} = 50\sqrt{N_i}$. The center of the distribution $\bar{J}_i$ has been taken as $\bar{J}_i = pN_i/2$, where the polarization p is set by the OH gradient via $p = \Delta_{\mathrm{OH}}/\Delta_{\mathrm{OH}}^{\mathrm{max}}$; here, $\Delta_{\mathrm{OH}}^{\mathrm{max}} = A_{\mathrm{HF}}/2 \approx 50\ \mu\mathrm{eV}$.

[32] M. J. A. Schuetz *et al.* (unpublished).

[33] Numerical evidence (for small systems) indicates that small deviations from perfect symmetry between the QDs still yield an entangled (mixed) steady state close to $|\xi_{\mathrm{ss}}\rangle$ [26].

[34] We estimate $\gamma_{\mathrm{eff}}^{-1} \approx 1$ s; this is compatible with the semiclassical approximation and in agreement with typical polarization time scales [14,35].

[35] R. Takahashi, K. Kono, S. Tarucha, and K. Ono, Phys. Rev. Lett. **107**, 026602 (2011).

[36] H. Christ, J. I. Cirac, and G. Giedke, Phys. Rev. B **75**, 155324 (2007).

[37] The results obtained within this approximative factorization scheme have been confirmed by numerical simulations for small sets of nuclei [32].

[38] H. Bluhm, S. Foletti, D. Mahalu, V. Umansky, and A. Yacoby, Phys. Rev. Lett. **105**, 216803 (2010).

[39] M. Pioro-Ladrière, T. Obata, Y. Tokura, Y.-S. Shin, T. Kubo, K. Yoshida, T. Taniyama, and S. Tarucha, Nat. Phys. **4**, 776 (2008).

[40] G. Petersen, E. A. Hoffmann, D. Schuh, W. Wegscheider, G. Giedke, and S. Ludwig, Phys. Rev. Lett. **110**, 177602 (2013).

[41] J. Petta, J. Taylor, A. Johnson, A. Yacoby, M. Lukin, C. Marcus, M. Hanson, and A. Gossard, Phys. Rev. Lett. **100**, 067601 (2008).

[42] Note that any initial OH splitting $\bar{\omega}_{\mathrm{OH}}$ is damped to zero in the steady state [32].

[43] For fast recharging of the DQD, $\Gamma = \Gamma_R/2$, where Γ_R is the sequential tunneling rate to the right lead [26].